Large deformations of planar extensible beams and pantographic lattices: Heuristic homogenisation, experimental and numerical examples of equilibrium

F Dell 'Isola, I Giorgio, M Pawlikowski, Nicola Rizzi

Large deformations of planar extensible beams and pantographic lattices: Heuristic homogenisation, experimental and numerical examples of equilibrium

F. dell'Isola, I. Giorgio, M. Pawlikowski and N. L. Rizzi

November 13, 2015

Abstract

The aim of this paper is to find a computationally efficient and predictive model for the class of systems that we call "pantographic structures". The interest in these materials was increased by the possibilities opened by the diffusion of technology of 3D printing. They can be regarded, once choosing a suitable length scale, as families of beams (also called fibres) interconnected each other by pivots and undergoing large displacements and large deformations. There are, however, relatively few results in the literature of non-linear beam theory "ready-to-use". In this paper, we consider a discretised springs model for extensible beams and propose a heuristic homogenisation technique of the kind first used by Piola to formulate a continuum fully non-linear beam model. The homogenised energy which we obtain has some peculiar and interesting features which we start to describe by solving numerically some exemplary deformation problems. Furthermore, we consider pantographic structures, find the corresponding homogenised second gradient deformation energies and study some planar problems. Numerical solutions for these 2D problems are obtained via minimisation of energy and are compared with some experimental measurements, in which elongation phenomena cannot be neglected.
Keywords: Non-linear beam; Elastic surface theory; Second gradient models.

1 Introduction

In this paper we formulate a computationally efficient and predictive model for the class of pantographic structures presented in [1] where the experimental evidence is proven to be only in a partial agreement with the predictions obtained with available theoretical models [2–6]. These pantographic structures are constituted by two families of beams —which we sometimes call also fibres— interconnected, when intersecting each other, by elastic pivots (see the self-explicative Fig. 1): i.e. pivots which allow for relative rotations at the expense of some deformation energy. These fibres are forming an angle of $\pi/2$ in the reference configuration and the whole pantographic structure (and its constituting beams) can undergo large displacements and large deformations. While it is possible to find already in many technological artefacts (see e.g. [7]) or biological tissues (see e.g. [8–11]) some fabrics whose behaviour can be somehow assimilated to the one shown by pantographic micro-structures actually the materials having a pantographic microstructure have been conceived (see [12, 13]) on the basis of purely theoretical considerations aiming to prove the possibility of designing materials exhibiting some specific exotic mechanical behaviour. More specifically, in the last mentioned papers the intent was to prove that it is possible to imagine and design materials whose deformation energy depends exclusively on the second gradient of displacement. Subsequently the practical interest in these materials has been increased by the possibilities opened by the diffusion of technology of 3D printing.

As a matter of facts, only when the beams constituting the considered pantographic structures can be assumed to be inextensible, the theoretical models in [2–4] can be effectively applied. On the other hand, the experimental evidence undoubtedly indicates that the hypothesis of inextensibility cannot be assumed to be valid when the specific pantographic structures considered in [1] are subjected to an extensional bias test in the direction at $\pi/4$ (in the reference configuration) with respect to both fibres orientations. The models assuming the inextensibility of fibres are careful enough to describe

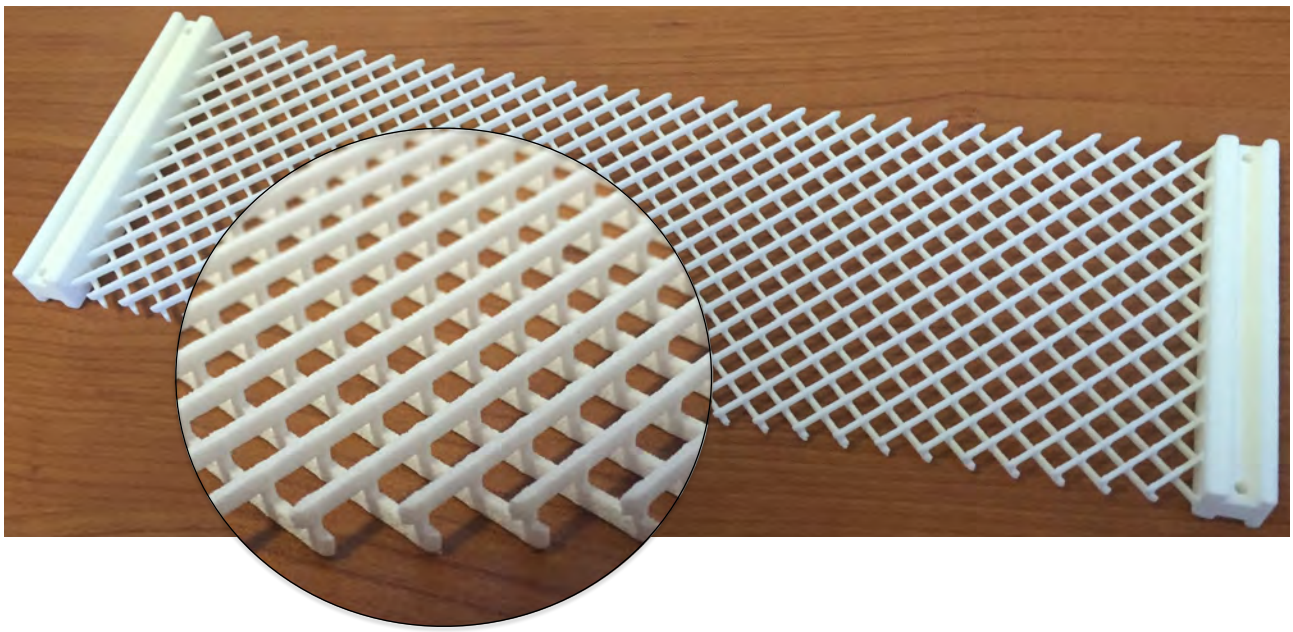

Figure 1: Pantographic lattice topology.

qualitatively the shapes assumed by pantographic sheets undergoing the extensional bias test but they fail in supplying accurate quantitative predictions: they only account for fibres bending energy and for elastic energy stored in the interconnecting pivots while they are completely neglecting fibres extensional energy. Therefore, the present paper is devoted to the formulation of a model in which such last fibres deformation energy is carefully accounted for. At this point, for the sake of self-consistency of the presentation, some considerations are needed concerning the different models which can and are, in fact, introduced for pantographic structures. One could choose to model considered pantographic structures at a relatively small length scale. To be specific: a small length scale which is able to allow for the precise description of the geometry of the elastic pivots, their mechanical properties and their deformation. Such high resolution models could be obtained by means of a micro-model based on Cauchy first gradient continuum theories: these last will imply the use of some related numerical models involving finite elements schemes with several millions of degrees of freedom also for relatively small specimens as those considered in the measurements presented in [1]. The heavy computational burden of such models makes their use, at least in the mid term horizon and considered the state of the art of contemporary computing technology, absolutely inappropriate. We, therefore, are motivated to present a higher-gradient reduced order-model leading to a rather more effective numerical modelling whose predictive performances (as will be shown in a forthcoming paper in preparation: Giorgio I, et al. *Numerical identification procedure between a micro Cauchy model and a macro second gradient model for planar pantographic structures.*) are however absolutely comparable to aforementioned more refined ones. This macro-model will be characterised by a length scale in which the elastic pivots have negligible dimensions, even if the considerable amount of deformation energy which they elastically store will actually be accounted for by means of the introduction of a constitutive prescription of a suitable shear deformation elastic constant (see following Eq. (30)). The other mechanical properties of pantographic lattices in planar motion will be accounted for by means of two other constitutive parameters: one representing extensional stiffness of modelled fibres and the other allowing for the consideration of their bending stiffness. We will show that such a simplified constitutive modelling is possible also when considering large displacements and large deformations of pantographic structures. The macro-model which we introduce in the present paper is used, by means of standard FEM, to get effective numerical simulations which are very predictive. Usually to deal with two-dimensional second gradient continua in a numerical context, Argyris elements are employed because, having C^1 continuity, they can be used to properly approximate solutions in the Sobolev space H^2 as required by this kind of problems. However, we did not use this kind of elements in order to perform simulation

in a more general FEA framework, as explained in Sect. 3.2, in view of application to 3D continua of results obtained herein. One should, nevertheless, remark that higher gradient continuum models do require novel integration schemes, more suitable to their intrinsic and more complicated structure: there are indeed impressive results indicating that isogeometric methods may further increase the numerical effectiveness of the reduced models we present here, especially when completely spatial models will be considered (see e.g. [14–20]). The problem of micro-macro model identification is one of the most formidable challenge in modern mathematical physics. Gamma convergence methods applied e.g. in [21–24] or the more classical strong convergence methods employed e.g. in [28] present remarkable technical difficulties and are not able to supply, in a constructive way, the limit-continuum-homogenised macro-model corresponding to a given discrete micro-model. In fact, the macro model must be conjectured via a suitable heuristic argument (as those used in [6, 24–27]) and only when both macro and micro models have been formulated and their properties are carefully studied then an effort to prove the convergence of a family of micro-models, as parametrised with a suitable length scale, to the independently conjectured macro model can be effectively tried.

Already in [29] a heuristic micro-macro identification procedure (to our knowledge for the first time) is introduced. By means of this procedure Piola manages to formulate (again for the first time) the theory of generalised continua and also the continuum models which have been recently renamed as Peridynamics (see [30]). Piola's heuristic homogenisation method is based on the following steps: i) the postulation of a micro-macro kinematical map, ii) the identification of micro and macro virtual work functionals and iii) the consequent determination of macro-constitutive equations in terms of the micro properties of considered mechanical systems by means of a suitable formal asymptotic expansion. Piola uses, following the rigour standards of his time, a mathematical deduction process in which micro-placement fields of material particles situated in the nodes of a referential lattice are calculated by means of the values in such nodes of a suitably regular macro-placement field and their gradients, by assuming that suitable Taylor expansions produce acceptable approximations. The heuristic identification procedure presented here follows exactly the spirit of Piola's work (see the following formulas (4), (5) and (20)). It has also to be remarked that in his works Gabrio Piola also considers separately one dimensional, two dimensional and three dimensional continua as continua whose reference configuration is —respectively— a curve, a surface or a regular connected subset having non vanishing volume embedded in the Euclidean three dimensional space. This subdivision of the presented matter was later followed by Cosserat Brothers [31, 32]: how to detect the influence on their works exerted by Piola's pioneering ones is a historical problem which deserves further in-depth studies [33].

In the present paper, differently from what done in [29] where the micro-macro identification is obtained by identifying micro with macro virtual work functionals, we identify macro-deformation energy, i.e. a macroscopic Lagrangian (line or surface) density of deformation energy, in terms of constitutive parameters appearing in the postulated expressions of micro-deformation energies. Our heuristic homogenisation procedure is applied first for a class of non-linear one-dimensional continua (beams), focusing on modelling phenomena in which both extensional and bending deformations are of relevance, and subsequently for the class of two-dimensional continua studied in [5]): in both cases we limit our attention to planar motions. In fact, there are relatively few results in the literature of non-linear beam theory: we recall here the very first classical results by Euler and Bernoulli [34] and the researches stemming from von Kármán [35, 36] for moderately large rotations but small strains. Moreover, very often in the literature, the simultaneous extension and bending deformation for non-linear beams are not considered: however when considering two dimensional continua embedding families of fibres (see e.g. the models presented in [2–4]) as a model of some specific micro-structured mechanical systems (as fabrics or pantographic sheets see e.g. [1, 7, 37]) the assumption that the fibres cannot extend while bending is not phenomenologically well-grounded [1]. Moreover bending phenomena appear to be coupled with extensional ones. Therefore, we are led to focus our attention on some two dimensional continua in which the second gradient of in-plane displacement (involving so called geodesic bending see also [5, 38]) appears in the expression of deformation energy. To be more precise, the heuristic micro-macro identification which we present here is based on the introduction of a discrete meso-model for nonlinear beams or pantographic planar structures: we consider a set

of material particles arranged on a one-dimensional or two-dimensional lattice suitably connected by extensional springs. Moreover, at each node of the lattice (see subsequent Figs. 2 and 3) suitable rotational springs are introduced which are deformed when the angle formed by two contiguous extensional springs is changed. For the sake of simplicity, we limit our attention to pantographic structures having orthogonal fibres in the reference configuration. For different fibre configurations, the symmetry analysis performed in [39, 40] may be useful for postulating 2D or 3D strain energy densities. The discrete model which we consider here is not completely unknown in the literature, but it seems to us that its potentialities in the effective modelling of complex structures has not been fully exploited: it generalises for the case of extensible beams those described e.g. in [41–48]. Indeed we intend to model structures where extension and large displacements and deformations of constituting beams are of relevance. The homogenised energy which we obtain for Hencky-type beams has some peculiar features which we start to describe by solving numerically some exemplary deformation problems. In particular, to approximate the mechanical actions exerted on the most deformed beams in extensional bias test of pantographic structures (i.e. those beams at the boundary between blue and green regions in Fig. 15) we consider a deformation problem for a non-linear Hencky type beam interconnected with a continuos distribution of springs having non-constant elasticity coefficient (see Fig. 6). The modelling assumptions we introduce are based on a physically-reasonable discrete microstructure of the considered class of beams and pantographic structures and do apply to the case of large deformations. Actually, we generalise the treatment found in the literature as up to now these microstructures were assumed to be constituted by rotational springs and exclusively by rigid bars, and were used only to get discrete Lagrangian models being an approximation of continuum models in linearised regimes. The discretisation schemes considered were possibly applied to design analog computers (see e.g. [49, 50]) or for obtaining finite differences integration schemes (see e.g. [41–48]). To our knowledge only in the paper [51] the case of large displacements and large deformation has been already approached.

Some numerical solutions have been obtained for a set of exemplary planar equilibrium problems for pantographic structures by using standard FE packages of *COMSOL Multiphysics*®. The results of performed simulations are shown in Sect. 3 and some of them are compared with obtained experimental measurements. The experimental setting is the same as the one described in [1], however, the measurements presented here are based on the acquisition and elaboration of a larger set of data. Actually (see the following Fig. 11) by using an *ad hoc* acquisition card and software it has been possible to measure the actual position, for all extensional bias tests performed, of all physical nodes (corresponding to elastic pivots) labelled by a black dot. The large set of numerical data gathered has been perfectly described by the introduced second gradient 2D continuum model formulated in this paper, which needs the specification of only three constitutive parameters. Indeed the best fit of these three elasticity coefficients allows us, for instance, to describe in a unitary and predictive way the six extension tests shown in Fig. 15. The model is numerically very efficient and it allows for careful predictions with simulations lasting (in all considered planar cases) few minutes when using commercial (although suitably designed) workstations. In the conclusions, we indicate a list of some mathematical problems which seem to be worth of consideration. The natural development of the present work involves the study of spatial (three-dimensional) placements of one dimensional or two dimensional continua or the introduction of three dimensional continua embedding reinforcement fibres: of interest can be the study of pantographic 2D or 3D higher gradient continua in which fibres are not orthogonal straight lines in the reference configuration. Also the introduction of functionally graded elastic coefficients of introduced continua can lead to the description and the prediction of interesting phenomena and potential applications. Among future developments, the study of dynamic properties of pantographic structures may unveil very attractive and uncommon behaviours (see e.g. [52–54]). Moreover, the problem of formulating intermediate meso-models, involving a class of Generalised Beam Theories, must necessarily be confronted: for instance the deformation of beam sections involving warping, Poisson effects, elastic necking or large shear or twist deformation can definitively be studied via reduced order models (see e.g. [55–61]) without resorting to the most detailed micro Cauchy first gradient models. Finally a larger set of experimental data including the deformation tests of the type considered in the numerical simulations presented in Figs. 8, 9 and 10 is needed. We expect that they will be similarly described without the addition of further constitu-

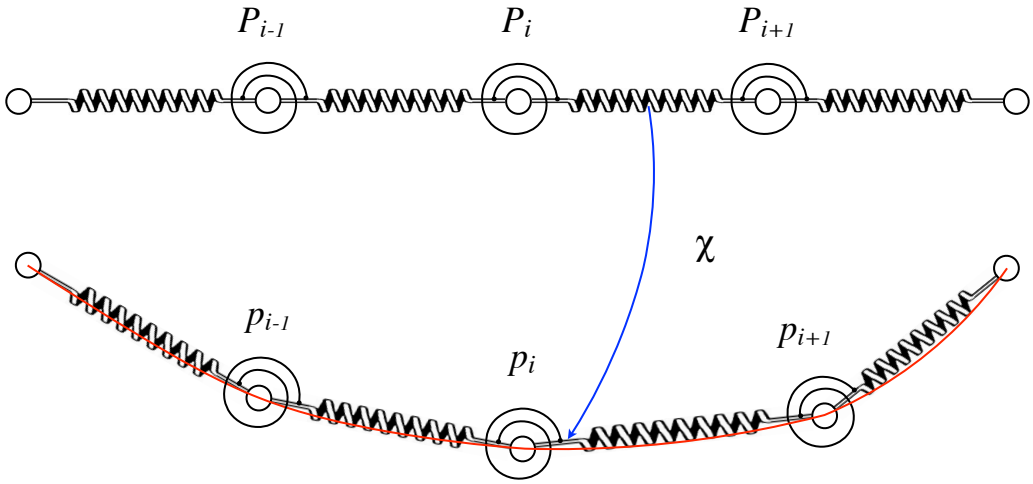

Figure 2: Micro-model and Piola identification: the red curve is the plot of the placement $\boldsymbol{\chi}$.

tive parameters. On the other hand, a larger number of constitutive parameters is expected when out-of-plane deformation tests are to be described. To identify these parameters, the method outlined in [62–66] can be profitably employed.

2 Macro-energies for non-linear beams and pantographic structures

Micro-macro identification process *à la Piola* produces a constitutive equation for macro-energy as a function of macro-placement field. The parameters involved in this constitutive equation become, thus, specified in terms of micro-mechanical properties of considered micro-structure. The main assumption on which Piola's procedure is based consists in the choice of the kinematical map: such a map specifies (in a rather arbitrary way) a unique micro-motion once a macro-motion is given. The influence of the kinematical map on macro-constitutive equations is often more important than the micro-constitutive equations and the geometric specifications of considered system at micro-level. Although this circumstance is often overlooked, the range of applicability of obtained macro models may depend dramatically on the properties of the kinematic map.

Therefore the heuristic deduction adopted here will need a rigorous justification on the basis of precise convergence criteria; such a justification, we will postpone to further investigations, on the basis of the promising results which we present here. We believe that their preliminary presentation seem to justify some more mathematically rigorous studies.

2.1 Micro-macro identification procedures: non-quadratic second gradient continuum energies

We present here first the identification procedure for considered class of extensible beams and secondly the identification procedure for an extensible pantographic lattice.

2.1.1 Identification for extensible beams

The presented heuristic micro-macro identification is performed under the following assumptions (see Fig. 2):

- the reference configuration of the discrete micro-system is constituted by masses placed at the points
$$\boldsymbol{P}_i := a_i\varepsilon \quad \text{where} \quad a_i = 0, 1, \dots, N;$$
- the current configuration of $\boldsymbol{P}_i$ will be denoted by $\boldsymbol{p}_i$;

- the generic pair of adjacent masses, at locations $(\boldsymbol{P}_i,\, \boldsymbol{P}_{i+1})$, is connected by a spring whose deformation energy depends on the distance between their present positions $\boldsymbol{p}_i$ and $\boldsymbol{p}_{i+1}$;
- at the node i a rotational spring is placed whose deformation energy depends on the angle ϑ_i formed by the vectors $\boldsymbol{p}_{i-1} - \boldsymbol{p}_i$ and $\boldsymbol{p}_{i+1} - \boldsymbol{p}_i$;
- the micro-Lagrangian discrete system having its configuration specified by the set of Lagrangian parameters $\{\boldsymbol{p}_i\}$ has the deformation energy given by

$$U(\{\boldsymbol{p}_i\}) = \sum_i \frac{k_i}{2} \left(\left\| \boldsymbol{p}_{i+1} - \boldsymbol{p}_i \right\| - \varepsilon \right)^2 + \sum_i b_i \left(\cos \vartheta_i + 1 \right) \tag{1}$$

where

$$\left\| \boldsymbol{p}_{i+1} - \boldsymbol{p}_i \right\| = \sqrt{(\boldsymbol{p}_{i+1} - \boldsymbol{p}_i) \cdot (\boldsymbol{p}_{i+1} - \boldsymbol{p}_i)} \tag{2}$$

and

$$\cos \vartheta_i = \frac{(\boldsymbol{p}_{i-1} - \boldsymbol{p}_i) \cdot (\boldsymbol{p}_{i+1} - \boldsymbol{p}_i)}{\left\| \boldsymbol{p}_{i-1} - \boldsymbol{p}_i \right\| \left\| \boldsymbol{p}_{i+1} - \boldsymbol{p}_i \right\|} \tag{3}$$

- as a macro model of the mass-spring system described before, we consider a 1D continuum whose reference configuration is given by the straight segment $\mathscr{I} = [0,\, L] \subset \mathbb{R}$, where $L = N\varepsilon$;
- the variable in the interval $\mathscr{I}$ is denoted by the abscissa S;
- planar motion: the macro-placement is described by the planar field

$$\boldsymbol{\chi} : [0,\, L] \to \mathbb{R}^2$$

Following the Piola's Ansatz we put

$$\boldsymbol{\chi} : \boldsymbol{P}_i \mapsto \boldsymbol{p}_i \tag{4}$$

and

$$\boldsymbol{\chi}(\boldsymbol{P}_{i+1}) = \boldsymbol{\chi}(\boldsymbol{P}_i) + \varepsilon \boldsymbol{\chi}'(\boldsymbol{P}_i) + \frac{\varepsilon^2}{2} \boldsymbol{\chi}''(\boldsymbol{P}_i) + o(\varepsilon^2) \tag{5}$$

where the $()'$ denotes derivative with respect to S. Using Eq. (5), Eq. (2) and Eqs. (2) and (3) can be rewritten as

$$\left\| \boldsymbol{p}_{i+1} - \boldsymbol{p}_i \right\| = \left\| \boldsymbol{\chi}'(\boldsymbol{P}_i) \right\| \varepsilon + \frac{\boldsymbol{\chi}'(\boldsymbol{P}_i) \cdot \boldsymbol{\chi}''(\boldsymbol{P}_i)}{\left\| \boldsymbol{\chi}'(\boldsymbol{P}_i) \right\|} \frac{\varepsilon^2}{2} + o(\varepsilon^2) \tag{6}$$

$$\cos \vartheta_i = \frac{\left[-\boldsymbol{\chi}'\left(P_i\right) + \boldsymbol{\chi}''\left(P_i\right) \frac{\varepsilon}{2} + o(\varepsilon^2) \right] \cdot \left[\boldsymbol{\chi}'\left(P_i\right) + \boldsymbol{\chi}''\left(P_i\right) \frac{\varepsilon}{2} + o(\varepsilon^2) \right]}{\left\| -\boldsymbol{\chi}'\left(P_i\right) + \boldsymbol{\chi}''\left(P_i\right) \frac{\varepsilon}{2} + o(\varepsilon^2) \right\| \left\| \boldsymbol{\chi}'\left(P_i\right) + \boldsymbol{\chi}''\left(P_i\right) \frac{\varepsilon}{2} + o(\varepsilon^2) \right\|} \tag{7}$$

$$\approx -1 + \left[\boldsymbol{c}_i \cdot \boldsymbol{c}_i - \left(\boldsymbol{e}_i \cdot \boldsymbol{c}_i \right)^2 \right] \frac{\varepsilon^2}{2} \tag{8}$$

where

$$\boldsymbol{e}_i = \frac{\boldsymbol{\chi}'\left(P_i\right)}{\left\| \boldsymbol{\chi}'\left(P_i\right) \right\|}, \qquad \boldsymbol{c}_i = \frac{\boldsymbol{\chi}''\left(P_i\right)}{\left\| \boldsymbol{\chi}'\left(P_i\right) \right\|} \tag{9}$$

The coefficient of the second-order term of series expansion (7) can be interpreted by means of the following equalities

$$\boldsymbol{c}_i \cdot \boldsymbol{c}_i - \left(\boldsymbol{e}_i \cdot \boldsymbol{c}_i \right)^2 = \boldsymbol{c}_i \cdot \boldsymbol{c}_i - \left(\boldsymbol{e}_i \cdot \boldsymbol{c}_i \right) \left(\boldsymbol{e}_i \cdot \boldsymbol{c}_i \right) = \left[\boldsymbol{c}_i - \left(\boldsymbol{e}_i \cdot \boldsymbol{c}_i \right) \boldsymbol{e}_i \right] \cdot \boldsymbol{c}_i = \boldsymbol{c}_{i\perp} \cdot \boldsymbol{c}_i = \boldsymbol{c}_{i\perp} \cdot \boldsymbol{c}_{i\perp} \tag{10}$$

where we denoted with the symbol $\boldsymbol{c}_{i\perp}$ the orthogonal projection of $\boldsymbol{c}_i$ onto the direction given by $\boldsymbol{e}_i$, i.e.

$$\boldsymbol{c}_{i\perp} := \boldsymbol{c}_i - \left(\boldsymbol{e}_i \cdot \boldsymbol{c}_i \right) \boldsymbol{e}_i. \tag{11}$$

Finally, Eq. (7) becomes:

$$\cos\vartheta_i + 1 \approx (\boldsymbol{c}_{i\perp} \cdot \boldsymbol{c}_{i\perp}) \frac{\varepsilon^2}{2}. \tag{12}$$

When representing the product $\boldsymbol{c}_{i\perp} \cdot \boldsymbol{c}_{i\perp}$ in terms of placement $\boldsymbol{\chi}$, we have

$$\boldsymbol{c}_{i\perp} \cdot \boldsymbol{c}_{i\perp} = \frac{\boldsymbol{\chi}''(P_i) \cdot \boldsymbol{\chi}''(P_i)}{\|\boldsymbol{\chi}'(P_i)\|^2} - \left(\frac{\boldsymbol{\chi}'(P_i) \cdot \boldsymbol{\chi}''(P_i)}{\|\boldsymbol{\chi}'(P_i)\|^2}\right)^2. \tag{13}$$

In conclusion, the energy (1) up to the second order terms in ε is represented as follows

$$U(\{\boldsymbol{p}_i\}) = \sum_i \frac{k_i\varepsilon^2}{2} \left(\|\boldsymbol{\chi}'(P_i)\| - 1\right)^2 + \sum_i \frac{b_i\varepsilon^2}{2} \left[\frac{\boldsymbol{\chi}''(P_i) \cdot \boldsymbol{\chi}''(P_i)}{\|\boldsymbol{\chi}'(P_i)\|^2} - \left(\frac{\boldsymbol{\chi}'(P_i) \cdot \boldsymbol{\chi}''(P_i)}{\|\boldsymbol{\chi}'(P_i)\|^2}\right)^2\right]. \tag{14}$$

When homogenizing via Piola's Ansatz and by rescaling the rigidities by means of the equations

$$k_i = K_e\varepsilon^{-1} \qquad b_i = K_b\varepsilon^{-1}$$

we get the following homogenized expression for deformation energy

$$U(\boldsymbol{\chi}(\cdot)) = \int_0^L \left\{\frac{K_e}{2} \left(\|\boldsymbol{\chi}'\| - 1\right)^2 + \frac{K_b}{2} \left[\frac{\boldsymbol{\chi}'' \cdot \boldsymbol{\chi}''}{\|\boldsymbol{\chi}'\|^2} - \left(\frac{\boldsymbol{\chi}' \cdot \boldsymbol{\chi}''}{\|\boldsymbol{\chi}'\|^2}\right)^2\right]\right\} \mathrm{d}S. \tag{15}$$

As a result, the action of considered system is

$$\mathscr{A}(\boldsymbol{\chi}(\cdot)) = \int_0^L \frac{1}{2}\varrho\dot{\boldsymbol{\chi}}^2 \mathrm{d}S - U(\boldsymbol{\chi}) \tag{16}$$

ϱ being the mass density per unit line.

It should be noted that $\boldsymbol{c}_\perp \cdot \boldsymbol{c}_\perp$ which appears in Eq. (15), when expressed in component form, coincides with the exact expression of the squared curvature, κ^2, of a beam which is axially deformable and shear undeformable reported in Appendix A. Besides, the squared Frenet curvature, k^2, of the beam axis in the present configuration, with some algebra from the definition [67], is related to the beam curvature $\kappa^2 = \boldsymbol{c}_\perp \cdot \boldsymbol{c}_\perp$ by the expression:

$$[k(S)]^2 = \frac{\boldsymbol{c}_\perp \cdot \boldsymbol{c}_\perp}{\|\boldsymbol{\chi}'(S)\|^2}. \tag{17}$$

2.1.2 Identification for extensible pantographic lattices

A very similar identification process holds for planar pantographic lattices we want to consider here.

Let us consider a Lagrangian Cartesian orthogonal coordinate system whose associated base of unit vectors is $(\mathbf{D}_1, \mathbf{D}_2)$. We assume that:

- in the reference configuration the lattice mass points are located at the positions

  $$\boldsymbol{P}_{i,j} := (a_i\varepsilon, a_j\varepsilon)$$

  where $a_i = 0, 1, \ldots, N$ and $a_j = 0, 1, \ldots, M$;
- the lattice dimensions result to be $L_1 = N\varepsilon$ and $L_2 = M\varepsilon$;
- the current configuration of $\boldsymbol{P}_{i,j}$ is denoted by $\boldsymbol{p}_{i,j}$;
- the masses at the nodes $\boldsymbol{P}_{i,j}$ are connected by extensional springs along each one of the coordinate lines;
- the energy of the extensional springs depends on the distance between two adjacent points, i.e. $\boldsymbol{p}_{i,j}$, $\boldsymbol{p}_{i+1,j}$ and $\boldsymbol{p}_{i,j}$, $\boldsymbol{p}_{i,j+1}$;

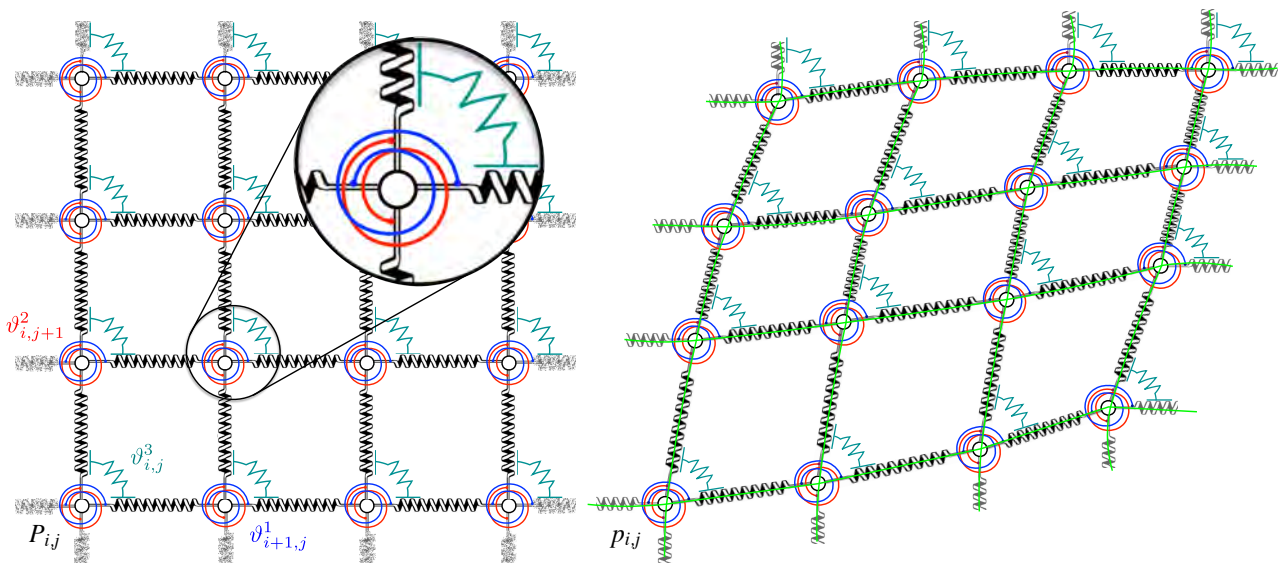

Figure 3: Micro-model of a pantographic sheet and Piola identification with a detail of the three rotational springs employed. The green curves are the plots of the placement $\boldsymbol{\chi}$.

- at each node there are two rotational springs, to provide bending rigidity along each coordinate line;
- the energy of the rotational springs depends on the angles: 1) $\vartheta^1_{i,j}$ formed by the vectors $\boldsymbol{p}_{i-1,j} - \boldsymbol{p}_{i,j}$ and $\boldsymbol{p}_{i,j} - \boldsymbol{p}_{i+1,j}$ and 2) $\vartheta^2_{i,j}$ formed by the vectors $\boldsymbol{p}_{i,j-1} - \boldsymbol{p}_{i,j}$ and $\boldsymbol{p}_{i,j+1} - \boldsymbol{p}_{i,j}$;
- in addition, at each node there is also a rotational spring between the two orthogonal lines;
- the deformation energy of these springs depends on the angle $\vartheta^3_{i,j}$ formed by the vectors $\boldsymbol{p}_{i,j+1} - \boldsymbol{p}_{i,j}$ and $\boldsymbol{p}_{i+1,j} - \boldsymbol{p}_{i,j}$.

As a result, by paralleling the assumptions made for a single chain of springs, to a lattice structure of springs (see Fig. 4 which exhibits two chains of springs arranged in the directions of fibers of a pantographic sheet), we will assume that for the micro-Lagrangian discrete system having its configuration specified by the set of Lagrangian parameters $\{\boldsymbol{p}_{i,j}\}$ the deformation energy is given by

$$
\begin{aligned}
U(\{\boldsymbol{p}_{i,j}\}) = &\sum_j \sum_i \frac{k^1_{i,j}}{2} \left(\left\|\boldsymbol{p}_{i+1,j} - \boldsymbol{p}_{i,j}\right\| - \varepsilon \left\|\mathbf{D}_1\right\|\right)^2 + \sum_j \sum_i b^1_{i,j} \left(\cos \vartheta^1_{i,j} + 1\right) \\
&+ \sum_i \sum_j \frac{k^2_{i,j}}{2} \left(\left\|\boldsymbol{p}_{i,j+1} - \boldsymbol{p}_{i,j}\right\| - \varepsilon \left\|\mathbf{D}_2\right\|\right)^2 + \sum_i \sum_j b^2_{i,j} \left(\cos \vartheta^2_{i,j} + 1\right) \\
&+ \sum_i \sum_j \frac{b^3_{i,j}}{2} \left|\vartheta^3_{i,j} - \frac{\pi}{2}\right|^\gamma
\end{aligned}
\tag{18}
$$

γ being a parameter which defines the shape of the function that characterises the pivot elastic potential. As a macro model of the mass-spring system described before we assume a 2D continuum whose reference configuration is given by a rectangle domain $\Omega = [0,\, L_1] \times [0,\, L_2] \subset \mathbb{R}^2$. The present configuration of Ω is described by the planar macro-placement

$$
\boldsymbol{\chi} : \Omega \to \mathbb{R}^2 \tag{19}
$$

via the following Piola's Ansatz

$$
\boldsymbol{\chi} : \boldsymbol{P}_{i,j} \mapsto \boldsymbol{p}_{i,j} \tag{20}
$$

$$
\left\|\boldsymbol{p}_{i+1,j} - \boldsymbol{p}_{i,j}\right\| = \left\|\boldsymbol{\chi}\left(P_{i+1,j}\right) - \boldsymbol{\chi}\left(P_{i,j}\right)\right\| \simeq \varepsilon \left\|\boldsymbol{F}\left(P_{i,j}\right) \mathbf{D}_1 + \frac{\varepsilon}{2} \nabla \boldsymbol{F}_{i,j} \left|\mathbf{D}_1 \otimes \mathbf{D}_1\right.\right\| \tag{21}
$$

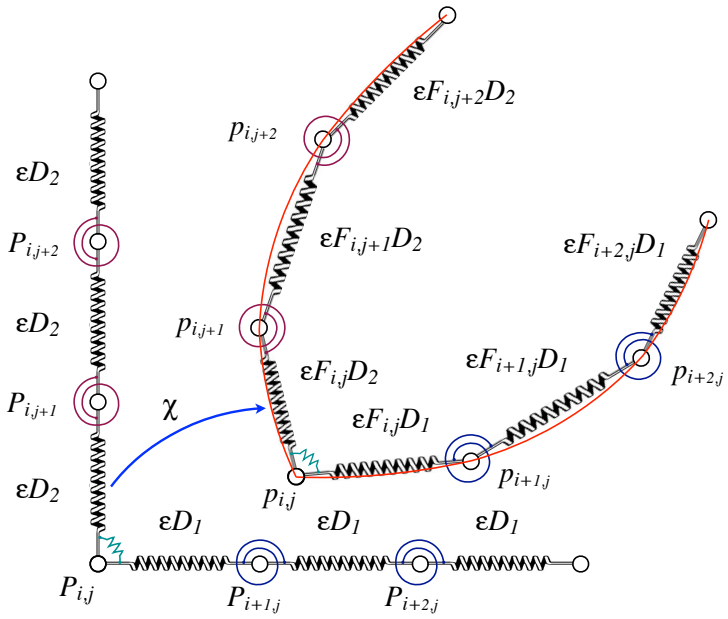

Figure 4: Micro-model of two fibers of a pantographic sheet.

and

$$\left\|\boldsymbol{p}_{i,j+1}-\boldsymbol{p}_{i,j}\right\| = \left\|\boldsymbol{\chi}\left(P_{i,j+1}\right)-\boldsymbol{\chi}\left(P_{i,j}\right)\right\| \simeq \varepsilon\left\|\boldsymbol{F}\left(P_{i,j}\right)\mathbf{D}_2+\frac{\varepsilon}{2}\nabla\boldsymbol{F}_{i,j}\left|\mathbf{D}_2\otimes\mathbf{D}_2\right.\right\| \tag{22}$$

where $\boldsymbol{F}=\nabla\boldsymbol{\chi}$ and $\left(\nabla\boldsymbol{F}\left|\mathbf{D}_\alpha\otimes\mathbf{D}_\alpha\right.\right)^\beta = F^\beta_{\alpha,\alpha}=\chi^\beta_{,\alpha\alpha}$; no sum over repeated α is indented. Besides, by introducing the notation $\boldsymbol{F}\left(P_{i,j}\right)=:\boldsymbol{F}_{i,j}$, we obtain for the angles related to the two families of fibers:

$$\cos\vartheta^\alpha_{i,j}\approx\frac{\left(-\boldsymbol{F}_{i,j}\mathbf{D}_\alpha+\frac{\varepsilon}{2}\nabla\boldsymbol{F}_{i,j}\left|\mathbf{D}_\alpha\otimes\mathbf{D}_\alpha\right.\right)\cdot\left(\boldsymbol{F}_{i,j}\mathbf{D}_\alpha+\frac{\varepsilon}{2}\nabla\boldsymbol{F}_{i,j}\left|\mathbf{D}_\alpha\otimes\mathbf{D}_\alpha\right.\right)}{\left\|-\boldsymbol{F}_{i,j}\mathbf{D}_\alpha+\frac{\varepsilon}{2}\nabla\boldsymbol{F}_{i,j}\left|\mathbf{D}_\alpha\otimes\mathbf{D}_\alpha\right.\right\|\left\|\boldsymbol{F}_{i,j}\mathbf{D}_\alpha+\frac{\varepsilon}{2}\nabla\boldsymbol{F}_{i,j}\left|\mathbf{D}_\alpha\otimes\mathbf{D}_\alpha\right.\right\|} \tag{23}$$

in which α denotes the fiber direction and, thus, takes value over the set $\{1,\,2\}$.

Moreover, the third angle $\vartheta^3_{i,j}$ can be evaluated by the expression:

$$\begin{aligned}\cos\vartheta^3_{i,j} &= \frac{\left[\boldsymbol{\chi}(\boldsymbol{P}_{i+1,j})-\boldsymbol{\chi}(\boldsymbol{P}_{i,j})\right]}{\|\boldsymbol{\chi}(\boldsymbol{P}_{i+1,j})-\boldsymbol{\chi}(\boldsymbol{P}_{i,j})\|}\cdot\frac{\left[\boldsymbol{\chi}(\boldsymbol{P}_{i,j+1})-\boldsymbol{\chi}(\boldsymbol{P}_{i,j})\right]}{\|\boldsymbol{\chi}(\boldsymbol{P}_{i,j+1})-\boldsymbol{\chi}(\boldsymbol{P}_{i,j})\|}\\ &\approx \frac{\boldsymbol{F}_{i,j}\mathbf{D}_1}{\|\boldsymbol{F}_{i,j}\mathbf{D}_1\|}\cdot\frac{\boldsymbol{F}_{i,j}\mathbf{D}_2}{\|\boldsymbol{F}_{i,j}\mathbf{D}_2\|}.\end{aligned} \tag{24}$$

Finally, by defining the following vectors

$$\boldsymbol{e}_{ij|\alpha}=\frac{\boldsymbol{F}_{i,j}\mathbf{D}_\alpha}{\|\boldsymbol{F}_{i,j}\mathbf{D}_\alpha\|},\qquad \boldsymbol{c}_{ij|\alpha}=\frac{\nabla\boldsymbol{F}_{i,j}\left|\mathbf{D}_\alpha\otimes\mathbf{D}_\alpha\right.}{\|\boldsymbol{F}_{i,j}\mathbf{D}_\alpha\|}\quad\text{with }\alpha=1,\,2 \tag{25}$$

and following the same steps taken for a single spring chain, we obtain:

$$\cos\vartheta^\alpha_{i,j}+1\approx\left(\boldsymbol{c}_{ij|\alpha\perp}\cdot\boldsymbol{c}_{ij|\alpha\perp}\right)\frac{\varepsilon^2}{2} \tag{26}$$

being, as the case treated before:

$$\begin{aligned}\boldsymbol{c}_{ij|\alpha\perp} &= \boldsymbol{c}_{ij|\alpha}-\left(\boldsymbol{e}_{ij|\alpha}\cdot\boldsymbol{c}_{ij|\alpha}\right)\boldsymbol{e}_{ij|\alpha}=\\ &= \frac{\nabla\boldsymbol{F}_{i,j}\left|\mathbf{D}_\alpha\otimes\mathbf{D}_\alpha\right.}{\|\boldsymbol{F}_{i,j}\mathbf{D}_\alpha\|}-\frac{\boldsymbol{F}_{i,j}\mathbf{D}_\alpha}{\|\boldsymbol{F}_{i,j}\mathbf{D}_\alpha\|}\left(\frac{\boldsymbol{F}_{i,j}\mathbf{D}_\alpha}{\|\boldsymbol{F}_{i,j}\mathbf{D}_\alpha\|}\cdot\frac{\nabla\boldsymbol{F}_{i,j}\left|\mathbf{D}_\alpha\otimes\mathbf{D}_\alpha\right.}{\|\boldsymbol{F}_{i,j}\mathbf{D}_\alpha\|}\right)\end{aligned} \tag{27}$$

and therefore

$$\boldsymbol{c}_{ij|\alpha\perp}\cdot\boldsymbol{c}_{ij|\alpha\perp}=\boldsymbol{c}_{ij|\alpha}\cdot\boldsymbol{c}_{ij|\alpha}-\left(\boldsymbol{e}_{ij|\alpha}\cdot\boldsymbol{c}_{ij|\alpha}\right)^2 \tag{28}$$

By rescaling the coefficients appearing in the energy (18) as follows

$$k^{\alpha}_{i,j}=K^{\alpha}_{e};\qquad b^{\alpha}_{i,j}=K^{\alpha}_{b};\qquad b^{3}_{i,j}=K_{p}\varepsilon^{2}; \tag{29}$$

we get, for the homogenised, the final expression:

$$\begin{aligned}U\left(\boldsymbol{\chi}\left(\cdot\right)\right)=&\int_{\Omega}\sum_{\alpha}\frac{K^{\alpha}_{e}}{2}\left(\|\boldsymbol{F}\mathbf{D}_{\alpha}\|-1\right)^{2}\mathrm{d}\Omega\\&+\int_{\Omega}\sum_{\alpha}\frac{K^{\alpha}_{b}}{2}\left[\frac{\nabla\boldsymbol{F}\left|\mathbf{D}_{\alpha}\otimes\mathbf{D}_{\alpha}\cdot\nabla\boldsymbol{F}\right|\mathbf{D}_{\alpha}\otimes\mathbf{D}_{\alpha}\right.}{\|\boldsymbol{F}\mathbf{D}_{\alpha}\|^{2}}-\left(\frac{\boldsymbol{F}\mathbf{D}_{\alpha}}{\|\boldsymbol{F}\mathbf{D}_{\alpha}\|}\cdot\frac{\nabla\boldsymbol{F}\left|\mathbf{D}_{\alpha}\otimes\mathbf{D}_{\alpha}\right.}{\|\boldsymbol{F}\mathbf{D}_{\alpha}\|}\right)^{2}\right]\mathrm{d}\Omega\\&+\int_{\Omega}\frac{K_{p}}{2}\left|\arccos\left(\frac{\boldsymbol{F}\,\boldsymbol{D}_{1}}{\|\boldsymbol{F}\,\boldsymbol{D}_{1}\|}\cdot\frac{\boldsymbol{F}\,\boldsymbol{D}_{2}}{\|\boldsymbol{F}\,\boldsymbol{D}_{2}\|}\right)-\frac{\pi}{2}\right|^{\gamma}\mathrm{d}\Omega\end{aligned} \tag{30}$$

3 Numerical simulations

Some numerical solutions for a set of exemplary planar equilibrium problems for beams and pantographic structures have been obtained using standard FEM packages in *COMSOL Multiphysics*. The approach is based on standard energy minimisation techniques. As the 1D and 2D continuum models obtained in Sect. 2 is of second gradient, we had to deal with the second derivatives of the displacement field. This problem has been handled by introducing an auxiliary kinematical field which takes the place of the displacement gradient (see e.g. [68–70]). In order to enforce the condition that the new field must be equal to the gradient of the displacement, the Lagrange multipliers technique has been used.

3.1 Some exemplary beam large deformation problems

In order to show some features of the proposed model, we consider the case of a cantilever beam when the free end is forced to move on a circular arch of radius $L/2$ and centre placed in the middle of the reference configuration. The results are reported in Fig. 5. There for five values of the displacement imposed to the free end the resulting configurations of the beam are exhibited. The beam has a length $L=1$ m, and is characterised by the following constitutive parameters:

- $K_e=4.05\times10^8$ N;
- $K_b=7.59\times10^5$ N m^2.

In a second example, a cantilever beam of length $L=1$ m lying on an elastic foundation, exerting reactions in both the directions horizontal and vertical, has been considered. The following cases have been examined.

case a The Winkler soil model is divided in two parts with the elastic constants: $K_{w1}=2.45\times10^8$ N/m^2, for $S\in[0,L/2)$ and $K_{w2}=8.2\times10^6$ N/m^2 for $S\in(L/2,L]$. Fixing the value of the bending stiffness $K_b=1.5\times10^4$ N m^2, the following sub-cases has been considered:

1. $K_{e1}=2.5\times10^7$ N
2. $K_{e2}=1.0\times10^9$ N

case b The Winkler constants are: $K_{w1}=8.2\times10^7$ N/m^2, for $S\in[0,L/2)$ and $K_{w2}=8.2\times10^7$ N/m^2 for $S\in(L/2,L]$. Now the value of the elongation stiffness $K_e=4.05\times10^8$ N, is fixed while two different values of K_b have been given, namely

1. $K_{b1}=100$ N m^2

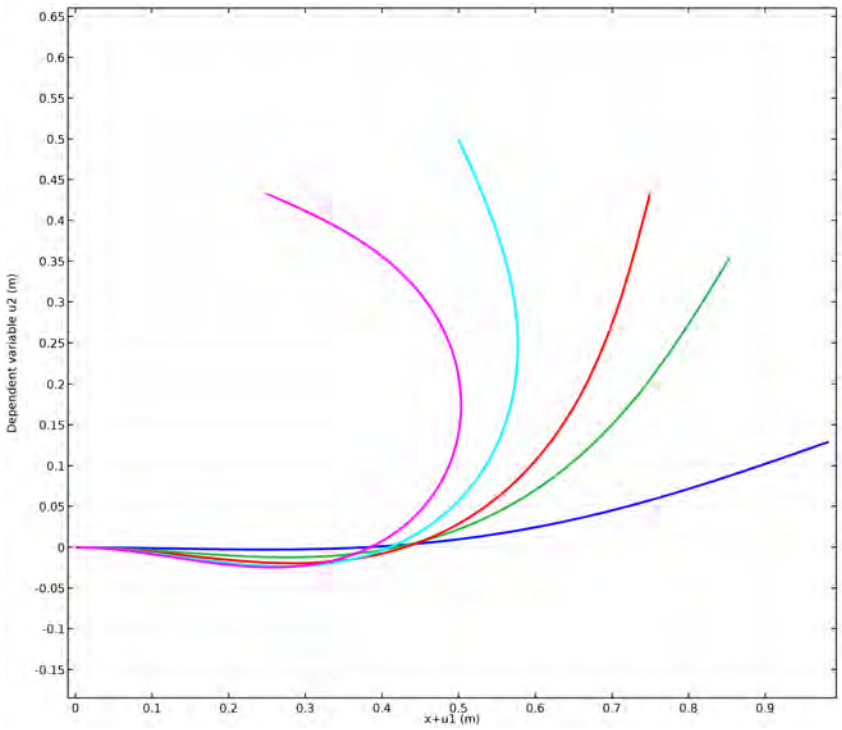

Figure 5: Large deflections of a cantilever beam.

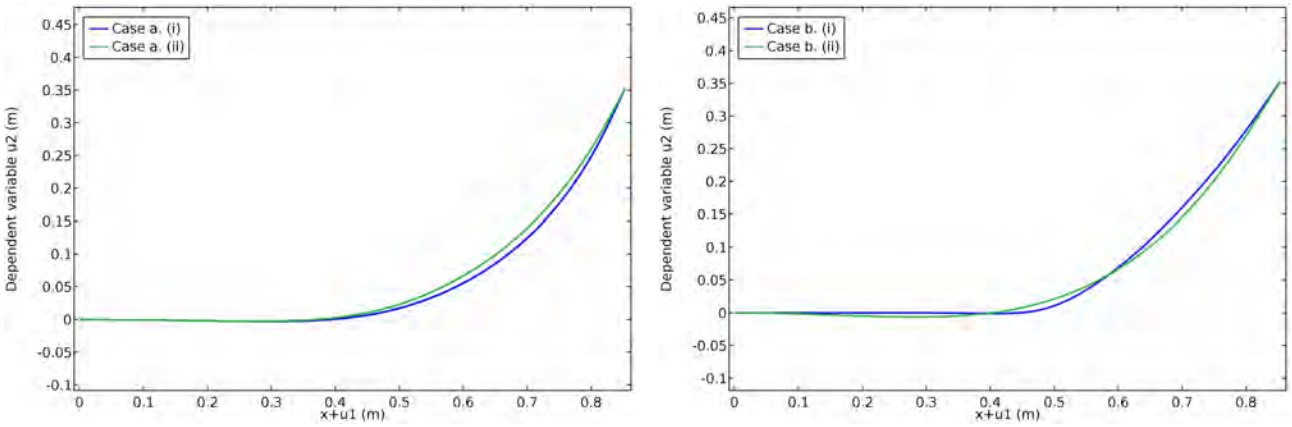

Figure 6: Beam on a Winkler spring model: case a (left), case b (right).

2. $K_{b2} = 1.5 \times 10^4$ N m^2

Figure 6 shows the current configurations of the beam under study for each one of the cases considered where the same displacement on the free end has been imposed.

On the left plot, it can be seen that increasing the value of the elongation stiffness, K_e, the length of the deformed beams decreases. Besides, the right plot shows that decreasing the bending stiffness, K_b, the curvature of the beam tends to localise near the point in which the Winkler constant changes.

3.2 Generalized large planar deformations for pantographic lattices and associated equilibrium energies

In this section some exemplary planar equilibrium problems for pantographic structures are performed. The results obtained are shown in Figs. 7, 8, 9 and 10 where the solid lines indicate the deformed shapes of the material lines which are straight in the reference configuration.

Let us consider the pantographic structure that in the reference configuration has the shape of a rectangle and let A, B, C, D be the position of its four vertices.

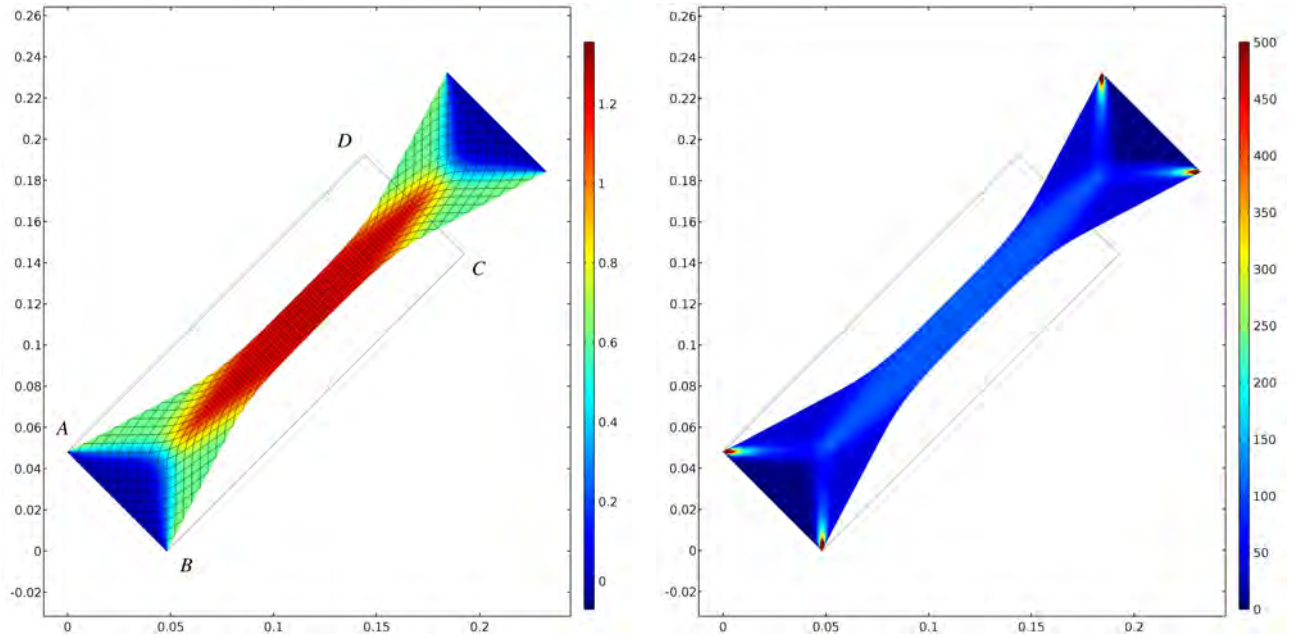

Figure 7: Numerical simulation of the bias extension test: colors indicate the shear strain relative to the initial fiber axes (left) and the strain energy density (rigth).

The following three cases have been examined:

case a standard extensional bias test – the edge AB is fixed while CD is translated by the vector $\beta(C-B)/\|C-B\|$;

case b the edge AB is fixed while CD is translated by the vector $\beta(D-C)/\|D-C\|$;

case c the edge AB is fixed, CD is translated by the vector $\beta(C-B)/\|C-B\|$ and is given an anticlockwise rotation ψ about its centre;

case d the edge AB is clockwise rotated of ψ about A while CD is rotated anticlockwise with the same amplitude about the point D; in addition CD is given a translation by the vector $\beta(A-D)/\|A-D\|$.

Fig. 7 shows the equilibrium configuration of the pantographic structure for case a) when $\beta = 0.0567$ m. Colours in the left picture exhibits the amplitude of shear strain relative to the initial fibre axes; the strain energy density is reported in the right picture.

Figs. 8, 9 and 10 show the equilibrium configurations of the structure under study. They also give information on strain energy density by means of colours. Specifically, Fig. 8 refers to case b) when three different amplitudes of the translation are given, that is $\beta = \{1, 3/2, 2\}\|D-C\|$; Fig. 9 displays the results for case c) when $\beta = \|D-C\|/2$ and $\psi = \{\pi/9, \pi/6, \pi/4\}$; Fig. 10 exhibits the results for case d) when $(\beta = 0, \psi = \pi/9)$, $(\beta = -\|D-C\|, \psi = \pi/9)$ and $(\beta = -3/2\|D-C\|, \psi = \pi/3)$.

4 Experimental evidence and comparison with numerical predictions

Experimental results and comparison with numerical simulation are presented in this section for a pantographic structure to illustrate the effectiveness of proposed models. The specimen under test has a rectangular shape whose sides are in ratio 1:3 and the long side has a length $L_1 = 0.2041$ m. The structure characterising the sample is made of two orthogonal families of 'beams' which are spaced 0.0048 m apart and connected by cylindrical pivots (see Fig. 11); it is built by means of a 3D printer and it is made of polyamide PA 2200 whose Young's modulus is about 1,600 MPa. The cross section of the elemental beams is 1.6×0.9 mm and it is the same for the two families. The pivots connecting the

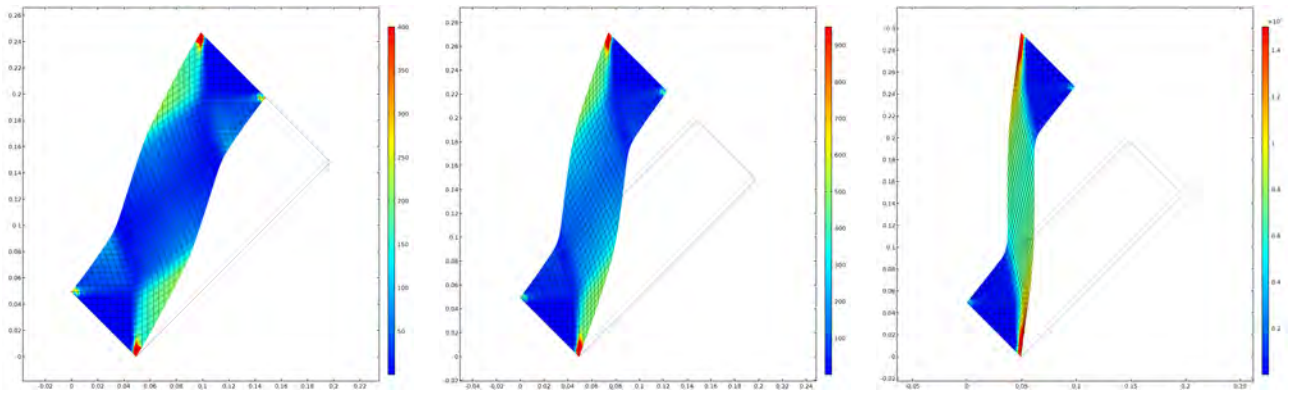

Figure 8: Case b: Equilibrium shape and strain energy density when a shear displacement is imposed.

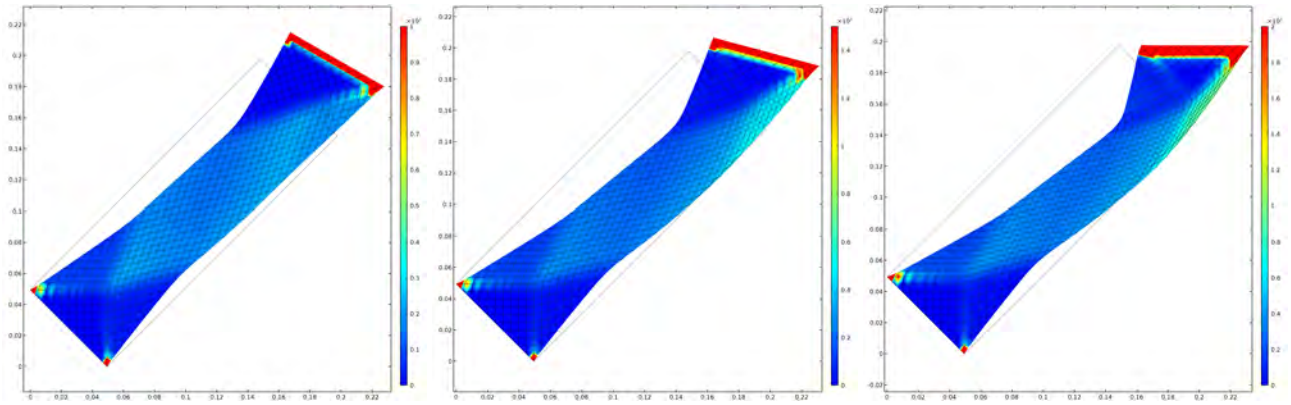

Figure 9: Case c: Equilibrium shape and strain energy density when a relative rotation and elongation of short sides is imposed.

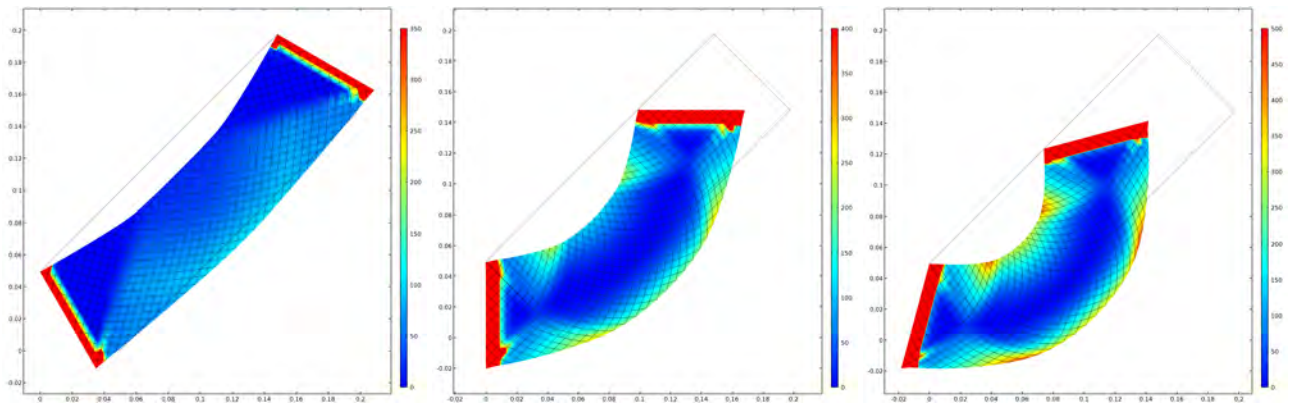

Figure 10: Case d: Equilibrium shape and strain energy density when a relative rotation and compression of short sides is imposed.

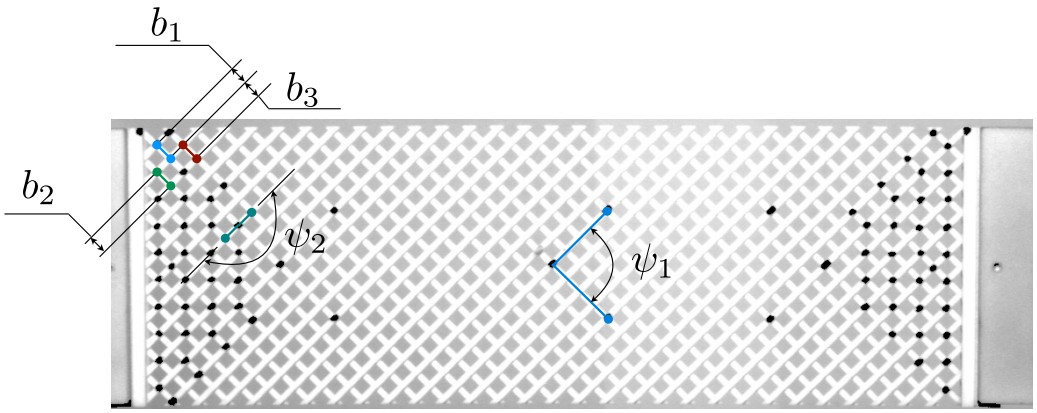

Figure 11: Specimen employed in tests and markers used for measurements.

two families of beams are characterise by a diameter of 0.9 mm and a height of 1.0 mm. A standard bias extension test was performed by means of the MTS Bionix test system at the rate 20 mm/min. Deformation was measured by means of a video extensometer on the same machine.
The material parameters characterising the behaviour of the structure under test, obtained by means of an identification procedure based on the proposed model (30), are summarised in Tab. 1.

Table 1: Identified material parameters

K_e (N m^{-1})	K_b (N m)	K_p (N m^{-1})	γ
1.34×10^5	1.92×10^{-2}	1.59×10^2	1.36

Figure 12 exhibits the measured angles ψ_1 and ψ_2 with the errors and the comparison with the numerical simulation performed with the identified parameters listed in Tab. 1. We choose these two angles because representative of the sample deformation; indeed, ψ_1 characterises the shear strain in the central region, while ψ_2 is distinctive of the most bended region (see Fig. 11). Fig. 12 shows clearly that the performed identification is consistent with the data accuracy.

Figure 13 depicts the measured force vs. the imposed displacement of the bias test and the corresponding data obtained by numerical simulations.

Figure 14 shows the relative elongations along the fibres related to two adjacent nodes at the corner of the sample; in particular, we consider the beam which converges into the corner ($b1$), the beam immediately neighbouring the inner side ($b2$), the beam neighbouring the outer side ($b3$). Also in this case measured data are compared with the relevant numerical simulations and are consistent with the data accuracy. In addition, it worth noting that the main axially deformation is related to the corner beam, $b1$, (about 6 %) while the other two beams appear to be almost axially undeformed. Therefore, a rather unusual localisation phenomenon of deformation is detected.

In Fig. 15 the equilibrium shapes of the sample under bias extension test are shown for different displacement imposed ($u = \{0.0143, 0.0232, 0.0321, 0.0411, 0.0500, 0.0567\}$ m) and compared with the corresponding shapes obtained by numerical simulations. The numerical results represent the current configuration of the material lines which in the reference configuration are superimposed to the straight beams of which the structure consists; the colours in plots indicate the decrease in the angle between $\boldsymbol{e}_1$ and $\boldsymbol{e}_2$ from the reference one, i.e. $\pi/2$. The model predicts an exotic arrangement of coexistent phases observed in the actual lattice in which the beams undergo part-wise uniform shears separated by internal transition layers due to the presence of the second gradient term in the stored energy proposed.

5 Conclusions and open problems

The pioneering works by Piola [29] and Hencky [41] continue to deserve the attention of the researchers in mathematical physics or in continuum and structural mechanics, especially in consideration of the

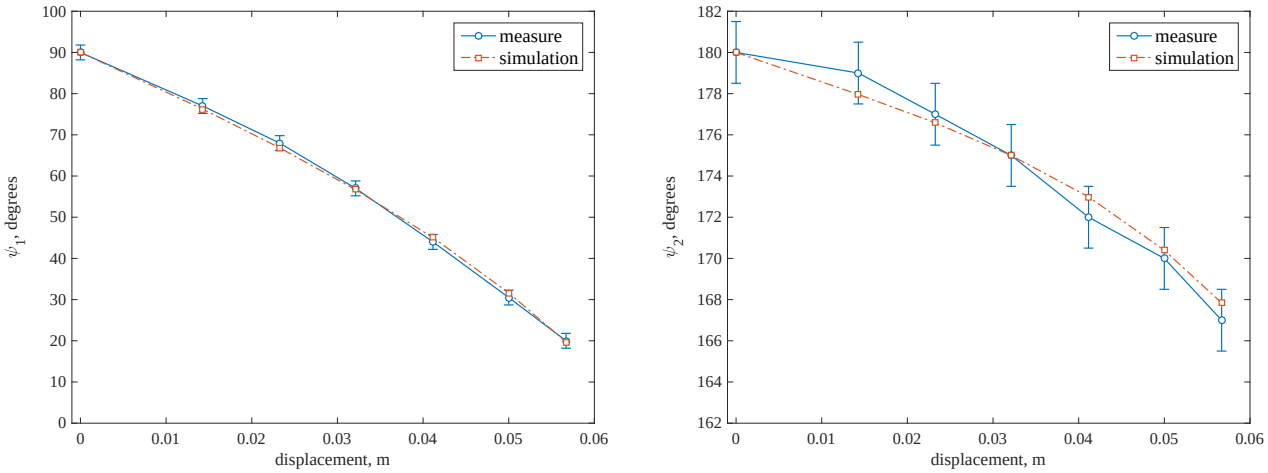

Figure 12: Angles used to identify the material parameters of Eq. (30) for the tested sample: ψ_1 (left) and ψ_2 (right).

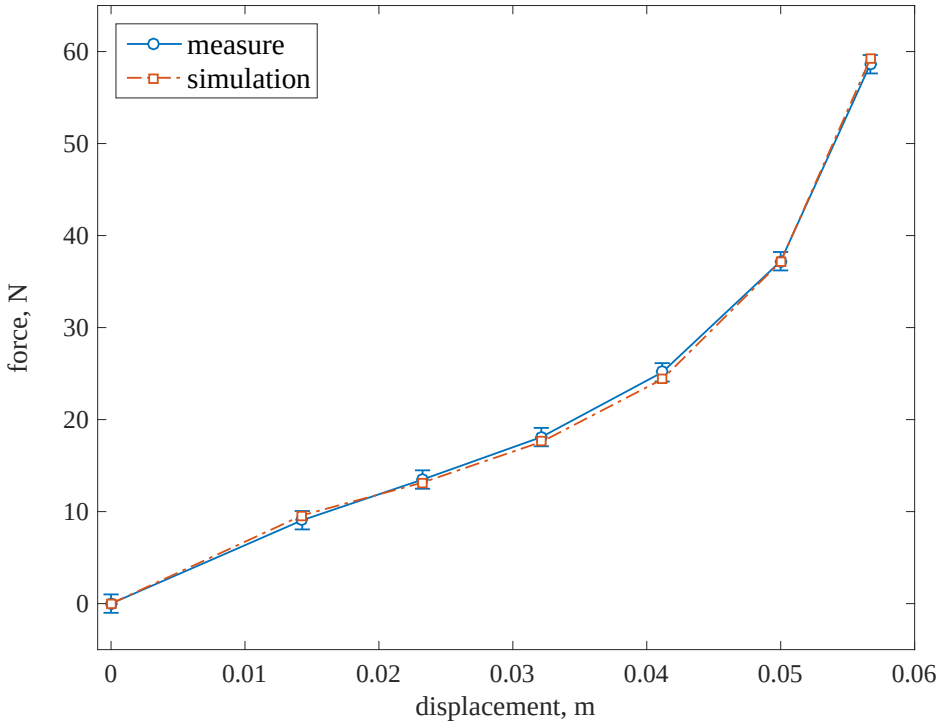

Figure 13: Force used to identify the material parameters of Eq. (30) for the tested sample.

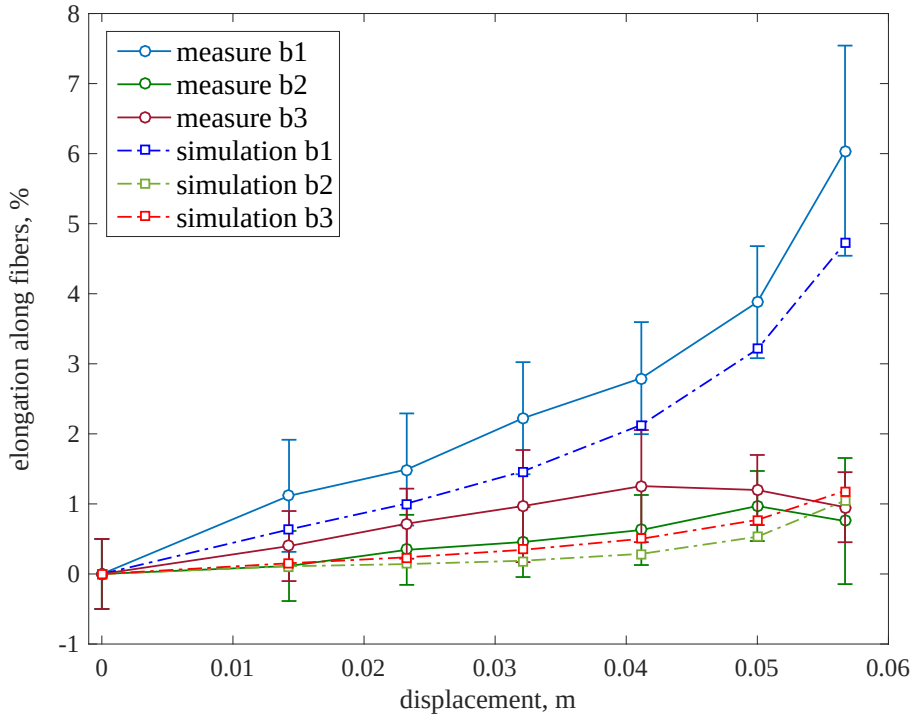

Figure 14: Elongations of three adjacent beams near a corner of the sample; comparison between measured data and simulations.

present effort to design and study exotic microstructure aimed to produce high performing materials or structures. The study and development of Smart or Optimised or Advanced or Multi-Physics and Multi-Scale Materials indeed require sophisticated mathematical tools: among these the calculus of variations plays a prominent role. The visionary results by Piola initiated the development of higher-gradient and weakly or strongly non-local continua (see [30, 33, 71–76]) while the ideas of Hencky introduced an efficient Lagrangian discretisation of continuum Euler-Bernoulli Beam Theory whose potential developments need still to be fully explored. The micro-structured materials which promise to open the way to new and unexpected technological applications (see [77]) demand for the formulation of computationally effective and really predictive models.

The results presented in this paper indicate, via the careful examination of a particular fabric for a recently designed metamaterial (see [1, 78–84]), i.e. pantographic structures that

1. standard Cauchy models are not easily applicable, at some length scales, to effectively describe — with a continuous model— those complex fabrics which show strong geometrical and mechanical inhomogeneities at smaller length scales;

2. a simple second gradient continuum model, deduced via homogenisation methods based on minimisation principles and techniques, is effective —at relatively larger scales— in modelling a large class of phenomena occurring during planar extensional bias test;

3. Hencky-type discrete models are effective also in suggesting generalised continuum models for complex materials.

It has to be remarked that some new mathematical problems need to be confronted when existence and uniqueness theorems are required for static and dynamic problems involving the non-quadratic second gradient energies introduced in Sect. 2. It indeed do not seem immediate to apply available mathematical techniques to prove well-posedness of the equilibrium or dynamical problems involving the deformation energies (15) or (30). Actually the set $\mathscr{C}$ constituted by the placement functions for which the deformation energy (15) is meaningful is necessarily included in the Sobolev space H^1 and includes obviously the Sobolev space H^2. However $\mathscr{C}$ does not coincide with any of them: its

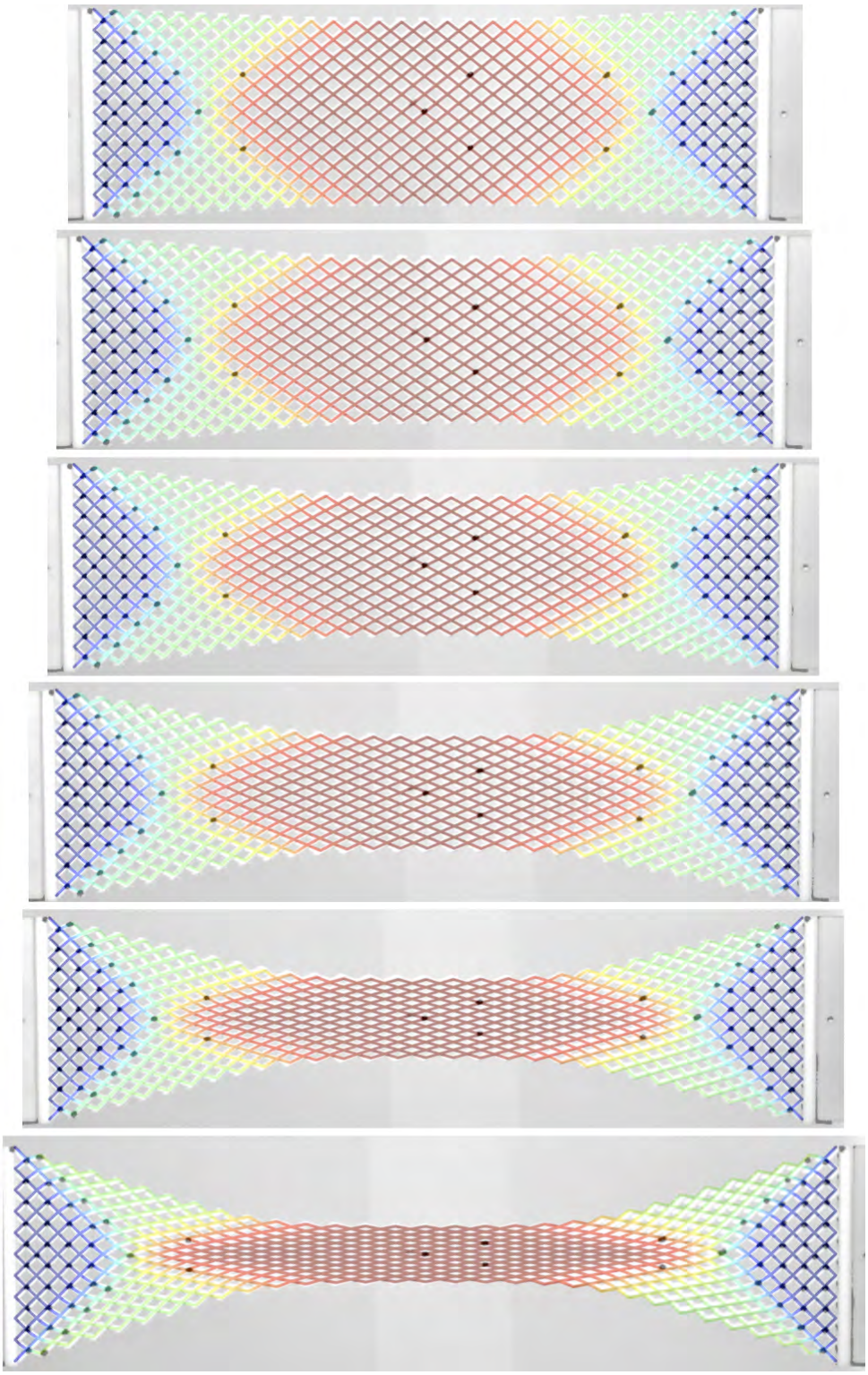

Figure 15: Overlap between simulation and measurement for six representative values of the displacement imposed.

structure needs to be determined in order to correctly formulate the equilibrium minimisation problem for considered Hencky-type non-linear beams. The situation becomes even more complex when the statics and the dynamics problems for pantographic structures are to be considered.

The relevance of aforementioned well-posedness problems in the study of considered micro-structures cannot be underestimated if only one thinks to the need of performing effective and complex numerical simulations in order to solve, for instance, optimisation problems.

The heuristic method presented here seems also adapted to generalise the study to the case of Hencky-type beams and 2D pantographic which move in the three-dimensional Euclidean space: we remark that it seems important the study of the problem of their wrinkling, buckling and post-buckling behaviour (see [85–91]). A first approach to this study has been already addressed, by introducing quadratic second gradient deformation energies only, in the papers [5, 38]: however, the experimental evidence seems to indicate that a complete theoretical picture of the significant phenomena occurring in the post-buckling of pantographic structures can be obtained only by introducing non-linearities also in the constitutive equations involving second gradient of displacements.

Finally the possibility of introducing three-dimensional pantographic micro-structures to design three-dimensional metamaterials has to be taken into account: the promising results presented here indicate that phenomena to be unveiled and the technological possibilities consequently to be opened could be of some relevance and interest.

A Appendix

Let us consider a straight segment $\mathcal{C}_0$ of length ℓ and denote by S its arc length so that the segment is described by the function

$$\boldsymbol{q}_0 : S \in [0, \ell] \to \boldsymbol{q}_0 \tag{31}$$

Let us consider a plane shape $\mathcal{R}$ and a point O on it.

Now attach a copy of $\mathcal{R}$ to each point of $\mathcal{C}_0$ through O so that $\mathcal{R}$ and $\mathcal{C}_0$ are orthogonal. We call $\mathcal{B}_0$ the reference configuration of a beam.

The present configuration $\mathcal{B}$ of $\mathcal{B}_0$ will be described by:

(a) the function $\boldsymbol{\chi}(S)$ i.e., the present position of $\boldsymbol{q}_0(S)$;

(b) a proper orthogonal tensor field $\mathbf{R}(S)$ i.e., the cross-sections rotation from $\mathcal{B}_0$ to $\mathcal{B}$.

Suitable strain measures (see e.g. [92]) are

$$\mathbf{E} = \mathbf{R}^\top \mathbf{R}' \tag{32}$$

$$\mathbf{e} = \mathbf{R}^\top \boldsymbol{\chi}' - \boldsymbol{q}_0' \tag{33}$$

where $()'$ denotes differentiation with respect to S. Now we assume a cartesian orthonormal coordinate frame with origin in $\boldsymbol{q}_0(0)$ and base $(\mathbf{D}_1 = \boldsymbol{q}_0', \mathbf{D}_2, \mathbf{D}_3)$.

In addition, we assume that $\boldsymbol{\chi}(S)$ remains in the span$\{\mathbf{D}_1, \mathbf{D}_2\}$, which in turn is orthogonal to the cross-sections, we can write

$$\boldsymbol{u} = \boldsymbol{\chi} - \boldsymbol{q}_0 = u_1 \mathbf{D}_1 + u_2 \mathbf{D}_2 \tag{34}$$

$$\mathbf{R} = \cos\varphi \mathbf{D}_1 \otimes \mathbf{D}_1 - \sin\varphi \mathbf{D}_1 \otimes \mathbf{D}_2 + \sin\varphi \mathbf{D}_2 \otimes \mathbf{D}_1 + \cos\varphi \mathbf{D}_2 \otimes \mathbf{D}_2 \tag{35}$$

and

$$\mathbf{e} = \varepsilon \mathbf{D}_1 + \gamma \mathbf{D}_2 \tag{36}$$

$$\mathbf{E} = \kappa(\mathbf{D}_2 \otimes \mathbf{D}_1 - \mathbf{D}_1 \otimes \mathbf{D}_2) \tag{37}$$

where

$$\begin{aligned}\varepsilon &= (1+u_1')\cos\varphi + u_2'\sin\varphi - 1\\ \gamma &= u_2'\cos\varphi - (1+u_1')\sin\varphi\\ \kappa &= \varphi'\end{aligned} \tag{38}$$

If the beam is assumed to be shear undeformable, we require

$$\begin{aligned}\gamma &\equiv 0 \Rightarrow u_2'\cos\varphi = (1+u_1')\sin\varphi\\ \gamma' &\equiv 0 \Rightarrow u_2''\cos\varphi - u_2'\varphi'\sin\varphi = u_1''\sin\varphi + (1+u_1')\varphi'\cos\varphi\end{aligned} \tag{39}$$

that give

$$\cos\varphi = \frac{1+u_1'}{\sqrt{u_2'^2+(1+u_1')^2}}, \quad \sin\varphi = \frac{u_2'}{\sqrt{u_2'^2+(1+u_1')^2}}$$
$$\kappa = \varphi' = \frac{u_2''(1+u_1') - u_2'u_1''}{u_2'^2+(1+u_1')^2} \tag{40}$$

References

[1] dell'Isola F, Lekszycki T, Pawlikowski M, Grygoruk R, Greco L. 2015 Designing a light fabric metamaterial being highly macroscopically tough under directional extension: first experimental evidence. *Z. Angew. Math. Phys.* (doi:10.1007/s00033-015-0556-4)

[2] Rivlin RS. 1997 Plane strain of a net formed by inextensible cords. In: *Collected Papers of RS Rivlin*, pp. 511–534. Springer, Berlin.

[3] Wang W-B, Pipkin AC. 1987 Plane deformations of nets with bending stiffness. *Acta Mech.* **65**, 263–279. (doi:10.1007/BF01176886)

[4] Steigmann DJ, Pipkin AC. 1991 Equilibrium of elastic nets. *Phil. Trans. R. Soc. Lond.* **335**, 419–454. (http://www.jstor.org/stable/53796)

[5] Steigmann DJ, dell'Isola F. 2015 Mechanical response of fabric sheets to three-dimensional bending, twisting, and stretching. *Acta Mech. Sinica* **31**, 373–382. (doi:10.1007/s10409-015-0413-x)

[6] Rahali Y, Giorgio I, Ganghoffer JF, dell'Isola F. 2015 Homogenization à la Piola produces second gradient continuum models for linear pantographic lattices. *Internat. J. Engrg. Sci.* **97**, 148–172. (doi:10.1016/j.ijengsci.2015.10.003)

[7] Ferretti M, Madeo A, dell'Isola F, Boisse P. 2014 Modeling the onset of shear boundary layers in fibrous composite reinforcements by second-gradient theory. *Z. Angew. Math. Phys.* **65**, 587–612. (doi:10.1007/s00033-013-0347-8)

[8] Grillo A, Federico S, Wittum G, Imatani S, Giaquinta G, Mićunović MV, 2009 Evolution of a fibre-reinforced growing mixture. *Nuovo cimento C* **32** 97–119. (doi:10.1393/ncc/i2009-10356-1)

[9] Grillo A, Federico S, Wittum G. 2012 Growth, mass transfer, and remodeling in fiber-reinforced, multi-constituent materials. *Int. J. Non-Linear Mech.* **47** 388–401. (doi:10.1016/j.ijnonlinmec.2011.09.026)

[10] Goda I, Assidi M, Ganghoffer JF. 2014 A 3D elastic micropolar model of vertebral trabecular bone from lattice homogenization of the bone microstructure. *Biomech. Model. Mechanobiol.* **13**, 53–83. (doi:10.1007/s10237-013-0486-z)

[11] Andreaus U, Giorgio I, Lekszycki T. 2014 A 2-D continuum model of a mixture of bone tissue and bio-resorbable material for simulating mass density redistribution under load slowly variable in time. *Z. Angew. Math. Mech.* **94**, 978–1000. (doi:10.1002/zamm.201200182)

[12] Alibert J-J, Seppecher P, dell'Isola F. 2003 Truss modular beams with deformation energy depending on higher displacement gradients. *Math. Mech. Solids* **8**, 51–73. (doi:10.1177/1081286503008001658)

[13] Seppecher P, Alibert J-J, dell'Isola F. 2011 Linear elastic trusses leading to continua with exotic mechanical interactions. *J. Phys. Conf. Ser.* **319**, 012018. (doi:10.1088/1742-6596/319/1/012018)

[14] Turco E, Aristodemo M. 1998 A three-dimensional B-spline boundary element. *Comput. Method. Appl. M.* **155**, 119–128. (doi:10.1016/S0045-7825(97)00147-3)

[15] Cazzani A, Malagù M, Turco E. 2014 Isogeometric analysis: a powerful numerical tool for the elastic analysis of historical masonry arches. *Contin. Mech. Thermodyn.* (doi:10.1007/s00161-014-0409-y)

[16] Cazzani A, Malagù M, Turco E. 2014 Isogeometric analysis of plane-curved beams. *Math. Mech. Solids* (doi: 10.1177/1081286514531265)

[17] Cazzani A, Malagù M, Turco E, Stochino F. 2015 Constitutive models for strongly curved beams in the frame of isogeometric analysis. *Math. Mech. Solids* (doi: 10.1177/1081286515577043)

[18] Cuomo M, Contrafatto L, Greco L. 2014 A variational model based on isogeometric interpolation for the analysis of cracked bodies. *Int. J. Eng. Sci.* **80**, 173–188. (doi:10.1016/j.ijengsci.2014.02.017)

[19] Greco L, Cuomo M. 2013 B-Spline interpolation of Kirchhoff–Love space rods. *Comput. Methods Appl. Mech. Eng.* **256**, 251–269. (doi:10.1016/j.cma.2012.11.017)

[20] Greco L, Cuomo M. 2014 An implicit G1 multi patch B-spline interpolation for Kirchhoff–Love space rod. *Comput. Methods Appl. Mech. Eng.* **269**, 173–197. (doi:10.1016/j.cma.2013.09.018)

[21] Alibert J-J, Della Corte A. 2015 Second-gradient continua as homogenized limit of pantographic microstructured plates: a rigorous proof. *Z. Angew. Math. Phys.* **66**, 2855–2870. (doi:10.1007/s00033-015-0526-x)

[22] Camar-Eddine M, Seppecher P. 2003 Determination of the closure of the set of elasticity functionals. *Arch. Ration. Mech. Anal.* **170** 211–245. (doi:10.1007/s00205-003-0272-7)

[23] Pideri C, Seppecher P. 1997 A second gradient material resulting from the homogenization of an heterogeneous linear elastic medium. *Contin. Mech. Thermodyn.* **9**, 241–257. (doi:10.1007/s001610050069)

[24] Boutin C. 1996 Microstructural effects in elastic composites. *Int. J. Solids Struct.* **33**, 1023–1051. (doi:10.1016/0020-7683(95)00089-5)

[25] Dos Reis F, Ganghoffer JF. 2014 Homogenized elastoplastic response of repetitive 2D lattice truss materials. *Comput. Mat. Sci.* **84**, 145–155. (doi:10.1016/j.commatsci.2013.11.066)

[26] Goda I, Assidi M, Ganghoffer JF. 2013 Equivalent mechanical properties of textile monolayers from discrete asymptotic homogenization. *J. Mech. Phys. Solids* **61**, 2537–2565. (doi:10.1016/j.jmps.2013.07.014)

[27] Dos Reis F, Ganghoffer JF. 2012 Construction of micropolar continua from the asymptotic homogenization of beam lattices. *Comp. Struct.* **112-113**, 354–363. (doi:10.1016/j.compstruc.2012.08.006)

[28] Carcaterra A, dell'Isola F, Esposito R, Pulvirenti M. 2015 Macroscopic description of microscopically strongly inhomogenous systems: a mathematical basis for the synthesis of higher gradients metamaterials. *Arch. Ration. Mech. Anal.* **218**, 1239–1262. (doi:10.1007/s00205-015-0879-5)

[29] dell'Isola F, Maier G, Perego U, Andreaus U, Esposito R, Forest S. 2014 The complete works of Gabrio Piola: Volume I - Commented English Translation. *Adv. Struct. Mater.* **38**, 1–813. (doi:10.1007/978-3-319-00263-7)

[30] dell'Isola F, Andreaus U, Placidi L. 2015 At the origins and in the vanguard of peridynamics, non-local and higher-gradient continuum mechanics: An underestimated and still topical contribution of Gabrio Piola. *Math. Mech. Solids* **20**, 887–928. (doi:10.1177/1081286513509811)

[31] Cosserat E, Cosserat F. 1896 Sur la théorie de l' élasticité. *Ann. Toulouse* **10**, 1–116.

[32] Cosserat E, Cosserat F. 1909 Théorie des corps déformables. Librairie Scientifique A. Hermann et Fils (engl. translation by D. Delphenich 2007), reprint 2009 by Hermann Librairie Scientifique, Paris.

[33] dell'Isola F, Esposito R, Della Corte A, Russo L. 2015 Some cases of unrecognized transmission of scientific knowledge: from antiquity to Gabrio Piola's peridynamics and generalized continuum theories. Submitted to *Adv. Struct. Mater.*

[34] Euler L. 1744 De curvis elasticis, Additamentum I to his Methodus inveniendi lineas curvas maximi minimive proprietate gaudentes. Lausanne and Geneva.

[35] Pai PF, Nayfeh AH. 1992 A nonlinear composite beam theory. *Nonlinear Dynam.* **3**, 273–303. (doi:10.1007/BF00045486)

[36] Heyliger PR, Reddy JN. 1988 A higher order beam finite element for bending and vibration problems. *J Sound Vib.* **126**, 309–326. (doi:10.1016/0022-460X(88)90244-1)

[37] dell'Isola F, Della Corte A, Greco L, Luongo A. 2015 Plane bias extension test for a continuum with two inextensible families of fibers: a variational treatment with Lagrange multipliers and a perturbation solution. *Int. J. Solids Struct.* (doi:10.1016/j.ijsolstr.2015.08.029)

[38] Giorgio I, Grygoruk R, dell'Isola F, Steigmann DJ. 2015 Pattern formation in the three-dimensional deformations of fibered sheets. *Mech. Res. Commun.* **69**, 164–171. (doi:10.1016/j.mechrescom.2015.08.005)

[39] Eremeyev VA, Pietraszkiewicz W. 2006 Local symmetry group in the general theory of elastic shells. *J. Elast.* **85**, 125–152. (doi:10.1007/s10659-006-9075-z)

[40] Eremeyev VA, Pietraszkiewicz W. 2012 Material symmetry group of the non-linear polar-elastic continuum. *Int. J. Solids Struct.* **49**, 1993–2005. (doi:10.1016/j.ijsolstr.2012.04.007)

[41] Hencky H. 1920 Über die angenäherte lösung von stabilitätsproblemen im raum mittels der elastischen gelenkkette. Der Eisenbau **11**, 437–452.

[42] Gambhir ML. 2004 Stability analysis and design of structures. Springer Science & Business Media, Berlin.

[43] Tůma J, Škutová J. 2012 Simulation of active vibration control of the cantilever beam. In: Carpathian Control Conference (ICCC), 2012 13th International. IEEE, pp. 744–747.

[44] Zhang Z, Wang CM, Challamel N, Elishakoff I. 2014 Obtaining Eringen's length scale coefficient for vibrating nonlocal beams via continualization method. *J. Sound Vib.* **333**, 4977–4990. (doi:10.1016/j.jsv.2014.05.002)

[45] Challamel N, Wang CM, Elishakoff I. 2014 Discrete systems behave as nonlocal structural elements: Bending, buckling and vibration analysis. *Eur. J. Mech. A-Solid.* **44**, 125–135. (doi:10.1016/j.euromechsol.2013.10.007)

[46] Challamel N, Lerbet J, Wang CM, Zhang Z. 2014 Analytical length scale calibration of non-local continuum from a microstructured buckling model. *Z. Angew. Math. Mech.* **94**, 402–413. (doi:10.1002/zamm.201200130)

[47] Challamel N, Zhang Z, Wang C. 2015 Nonlocal Equivalent Continua for Buckling and Vibration Analyses of Microstructured Beams. *J. Nanomech. Micromech.* **5**, A4014004. (doi:10.1061/(ASCE)NM.2153-5477.0000062)

[48] Wang CM, Zhang H, Gao RP, Duan WH, Challamel N. 2015 Hencky Bar-Chain Model for Buckling and Vibration of Beams with Elastic End Restraints. *Int. J. Str. Stab. Dyn.* **15**, 1540007. (doi:10.1142/S0219455415400076)

[49] Crandall SH, Karnopp DC, Kurtz EF, Pridmore-Brown DC. 1968 Dynamics of mechanical and electromechanical systems. McGraw-Hill.

[50] Giorgio I, Galantucci L, Della Corte A, Del Vescovo D. 2015 Piezo-electromechanical smart materials with distributed arrays of piezoelectric transducers: current and upcoming applications. *Int. J. Appl. Electromagn. Mech.* **47**, 1051–1084. (doi:10.3233/JAE-140148)

[51] Challamel N, Kocsis A, Wang CM. 2015 Discrete and non-local elastica. *Int. J. Non-Linear Mech.* **77**, 128–140. (doi:10.1016/j.ijnonlinmec.2015.06.012)

[52] Carcaterra A, Akay A, Bernardini C. 2012 Trapping of vibration energy into a set of resonators: Theory and application to aerospace structures. *Mech. Syst. Signal Pr.* **26**, 1–14. (doi:10.1016/j.ymssp.2011.05.005)

[53] Roveri N, Carcaterra A, Akay A. 2009 Energy equipartition and frequency distribution in complex attachments. *J. Acoust. Soc. Am.* **126**, 122–128. (doi:10.1121/1.3147502)

[54] Roveri N, Carcaterra A, Akay A. 2009 Vibration absorption using non-dissipative complex attachments with impacts and parametric stiffness. *J. Acoust. Soc. Am.* **126**, 2306–2314. (doi:10.1121/1.3212942)

[55] Luongo A, Zulli D. 2014 A non-linear one-dimensional model of cross-deformable tubular beam. *Int. J. Non-Linear Mech.* **66**, 33–42. (doi:10.1016/j.ijnonlinmec.2014.03.008)

[56] Piccardo G, Ranzi G, Luongo A. 2014 A complete dynamic approach to the generalized beam theory cross-section analysis including extension and shear modes. *Math. Mech. Solids* **19**, 900–924. (doi:10.1177/1081286513493107)

[57] Piccardo G, Ranzi G, Luongo A. 2014 A direct approach for the evaluation of the conventional modes within the GBT formulation. *Thin-Wall. Struct.* **74**, 133–145. (doi:10.1016/j.tws.2013.09.008)

[58] Ranzi G, Luongo, A. 2011 A new approach for thin-walled member analysis in the framework of GBT. *Thin-Wall. Struct.* **49**, 1404–1414. (doi:10.1016/j.tws.2011.06.008)

[59] Preumont A, Seto K. 2008 Active control of structures. John Wiley & Sons.

[60] Boubaker BB, Haussy B and Ganghoffer JF. 2007 Discrete models of woven structures. Macroscopic approach. *Compos. Part. B:Eng.* **38** 498–505. (doi:10.1016/j.compositesb.2006.01.007)

[61] Carassale L, Piccardo G. 2010 Non-linear discrete models for the stochastic analysis of cables in turbulent wind. *Int. J. Non-Linear Mech.* **45**, 219–231. (doi:10.1016/j.ijnonlinmec.2009.11.002)

[62] Placidi L, Andreaus U, Della Corte A, Lekszycki T. 2015 Gedanken experiments for the determination of two-dimensional linear second gradient elasticity coefficients. *Z. Angew. Math. Phys.* (doi: 10.1007/s00033-015-0588-9)

[63] Turco E. 2005 Is the statistical approach suitable for identifying actions on structures? *Comput. Struct.* **83**, 2112–2120. (doi:10.1016/j.compstruc.2005.03.006)

[64] Dietrich L, Lekszycki T, Turski K. 1998 Problems of identification of mechanical characteristics of viscoelastic composites. *Acta Mech.* **126**, 153–167. (doi:10.1007/BF01172805)

[65] Lekszycki T, Olhoff N, Pedersen JJ. 1992 Modelling and identification of viscoelastic properties of vibrating sandwich beams. *Compos. Struct.* **22**, 15–31. (doi:10.1016/0263-8223(92)90035-B)

[66] Solari G, Pagnini LC, Piccardo G. 1997 A numerical algorithm for the aerodynamic identification of structures. *J. Wind Eng. Ind. Aerod.* **69-71**, 719–730. (doi:10.1016/S0167-6105(97)00200-6)

[67] O'Neill B. 2006 Elementary Differential Geometry. Academic Press.

[68] Forest S. 2009 Micromorphic Approach for Gradient Elasticity, Viscoplasticity, and Damage. *J. Eng. Mech.* **135**, 117–131. (doi:10.1061/(ASCE)0733-9399(2009)135:3(117))

[69] Forest S, Cordero NM, Busso EP. 2011 First vs. second gradient of strain theory for capillarity effects in an elastic fluid at small length scales. *Comp. Mater. Sci.* **50**, 1299–1304. (doi:10.1016/j.commatsci.2010.03.048)

[70] Forest S, and Sievert R. 2006 Nonlinear microstrain theories. *Int. J. Solids Struct.* **43**, 7224–7245. (doi:10.1016/j.ijsolstr.2006.05.012)

[71] Placidi L. 2014 A variational approach for a nonlinear one-dimensional damage-elasto-plastic second-gradient continuum model. *Contin. Mech. Thermodyn.* (doi:10.1007/s00161-014-0405-2)

[72] Placidi L. 2015 A variational approach for a nonlinear 1-dimensional second gradient continuum damage model. *Contin. Mech. Thermodyn.* **27** 623–638. (doi:10.1007/s00161-014-0338-9)

[73] Rinaldi A, Placidi L. 2014 A microscale second gradient approximation of the damage parameter of quasi-brittle heterogeneous lattices. *Z. Angew. Math. Mech.* **94**, 862–877. (doi:10.1002/zamm.201300028)

[74] Yang Y, Ching W, Misra A 2011 Higher-Order Continuum Theory Applied to Fracture Simulation of Nanoscale Intergranular Glassy Film. *J. Nanomech. Micromech.* **1**, 60–71. (doi:10.1061/(ASCE)NM.2153-5477.0000030)

[75] Yang Y, Misra A. 2010 Higher-order stress-strain theory for damage modeling implemented in an element-free Galerkin formulation. *Comput. Model. Eng. Sci.* **64**, 1–36. (doi:10.3970/cmes.2010.064.001)

[76] Yang Y, Misra A. 2012 Micromechanics based second gradient continuum theory for shear band modeling in cohesive granular materials following damage elasticity. *Int. J. Solids Struct.* **49**, 2500–2514. (doi:10.1016/j.ijsolstr.2012.05.024)

[77] dell'Isola F, Steigmann DJ, Della Corte A. 2015 Synthesis of fibrous complex structures. Designing micro-structure to deliver targeted macro-scale response. Submitted to *Appl. Mech. Rev.*

[78] dell'Isola F, Giorgio I, Andreaus U. 2015 Elastic pantographic 2D lattices: a numerical analysis on the static response and wave propagation. *Proc. Est. Acad. Sci. Eng.* **64**, 219–225. (doi:10.3176/proc.2015.3.03)

[79] dell'Isola F, Della Corte A, Giorgio I, Scerrato D. 2015 Pantographic 2D sheets: discussion of some numerical investigations and potential applications. *Int. J. Non-Linear Mech.* (doi:10.1016/j.ijnonlinmec.2015.10.010)

[80] Frischmuth K, Kosiéski W, Lekszycki T. 1993 Free vibrations of finite-memory material beams. *Internat. J. Engrg. Sci.* **31**, 385–395. (doi:10.1016/0020-7225(93)90013-K)

[81] Del Vescovo D, Giorgio I. 2014 Dynamic problems for metamaterials: review of existing models and ideas for further research. *Internat. J. Engrg. Sci.* **80**, 153–172. (doi:10.1016/j.ijengsci.2014.02.022)

[82] Madeo A, Placidi L, Rosi G. 2014 Towards the design of metamaterials with enhanced damage sensitivity: Second gradient porous materials. *Res. Nondestruct. Eval.* **25**, 99–124. (doi:10.1080/09349847.2013.853114)

[83] Madeo A, Neff P, Ghiba ID, Placidi L, Rosi G. 2015 Band gaps in the relaxed linear micromorphic continuum. *Z. Angew. Math. Mech.* **95**, 880–887. (doi:10.1002/zamm.201400036)

[84] Neff P, Ghiba ID, Madeo A, Placidi L, Rosi G. 2014 A unifying perspective: The relaxed linear micromorphic continuum. *Contin. Mech. Thermodyn.* **26**, 639–681. (doi:10.1007/s00161-013-0322-9)

[85] Luongo A. 2001 Mode localization in dynamics and buckling of linear imperfect continuous structures. *Nonlinear Dynam.* **25** 133–156. (doi:10.1023/A:1012954700751)

[86] Luongo A, Zulli D and Piccardo G. 2009 On the effect of twist angle on nonlinear galloping of suspended cables. *Comput. & Structures* **87**, 1003–1014. (doi:10.1016/j.compstruc.2008.04.014)

[87] Ruta GC, Varano V, Pignataro M, Rizzi NL. 2008 A beam model for the flexural-torsional buckling of thin-walled members with some applications. *Thin-Wall. Struct.* **46**, 816–822. (doi:10.1016/j.tws.2008.01.020)

[88] Pignataro M, Rizzi NL, Ruta GC, Varano V. 2009 The effects of warping constraints on the buckling of thin-walled structures. *J. Mech. Mater. Struct.* **4**, 1711–1727. (doi:10.2140/jomms.2009.4.1711)

[89] Rizzi NL, Varano V. 2011. The effects of warping on the postbuckling behaviour of thin-walled structures. *Thin-Wall. Struct.* **49**, 1091–1097. (doi:10.1016/j.tws.2011.04.001)

[90] Gabriele S, Rizzi N, Varano V. 2012 On the imperfection sensitivity of thin-walled frames. *Civil-Comp Press* (doi:10.4203/ccp.99.15)

[91] Rizzi NL, Varano V, Gabriele S. 2013 Initial postbuckling behavior of thin-walled frames under mode interaction. *Thin-Wall. Struct.* **68**, 124–134. (doi:10.1016/j.tws.2013.03.004)

[92] Di Carlo A, Rizzi NL, Tatone A. 1990 One-dimensional continuum model of a modular lattice: identification of the constitutive functions for the contact and inertial actions. *Meccanica* **25**, 168–174. (doi:10.1007/BF01556436)